Hedgehog-responsive candidate cell of origin for diffuse intrinsic pontine glioma

Michelle Monje[a,b,c,1,2], Siddhartha S. Mitra[c,d,1], Morgan E. Freret[a,b,c], Tal B. Raveh[c], James Kim[b,c], Marilyn Masek[e], Joanne L. Attema[c,3], Gordon Li[d], Terri Haddix[e], Michael S. B. Edwards[d], Paul G. Fisher[a], Irving L. Weissman[c,e], David H. Rowitch[f,g], Hannes Vogel[e], Albert J. Wong[d,h], and Philip A. Beachy[b,c,2]

Departments of [a]Neurology, [b]Developmental Biology, [d]Neurosurgery, [e]Pathology, and [h]Cancer Biology, and [c]Institute for Stem Cell Biology and Regenerative Medicine, Stanford University Medical Center, Stanford, CA 94305; and Departments of [f]Neurological Surgery and [g]Pediatrics, University of California School of Medicine, San Francisco, CA 94143

Contributed by Philip A. Beachy, February 1, 2011 (sent for review July 28, 2010)

Diffuse intrinsic pontine gliomas (DIPGs) are highly aggressive tumors of childhood that are almost universally fatal. Our understanding of this devastating cancer is limited by a dearth of available tissue for study and by the lack of a faithful animal model. Intriguingly, DIPGs are restricted to the ventral pons and occur during a narrow window of middle childhood, suggesting dysregulation of a postnatal neurodevelopmental process. Here, we report the identification of a previously undescribed population of immunophenotypic neural precursor cells in the human and murine brainstem whose temporal and spatial distributions correlate closely with the incidence of DIPG and highlight a candidate cell of origin. Using early postmortem DIPG tumor tissue, we have established in vitro and xenograft models and find that the Hedgehog (Hh) signaling pathway implicated in many developmental and oncogenic processes is active in DIPG tumor cells. Modulation of Hh pathway activity has functional consequences for DIPG self-renewal capacity in neurosphere culture. The Hh pathway also appears to be active in normal ventral pontine precursor-like cells of the mouse, and unregulated pathway activity results in hypertrophy of the ventral pons. Together, these findings provide a foundation for understanding the cellular and molecular origins of DIPG, and suggest that the Hh pathway represents a potential therapeutic target in this devastating pediatric tumor.

Hedgehog pathway | cancer stem cells | brainstem glioma

Brainstem gliomas account for 10–20% of childhood brain tumors (1). Such tumors cluster into two disparate groups with widely divergent outcomes. Gliomas of the ventral pons (basis pontis), hereafter referred to as diffuse intrinsic pontine gliomas (DIPGs) (Fig. 1*A*), are typically diffusely infiltrative, higher grade [World Health Organization (WHO) II–IV], extremely aggressive cancers, leading to death in less than a year. Those arising in the dorsal pons (pontine tegmentum), midbrain, or medulla, in contrast, tend to be low-grade gliomas (often pilocytic astrocytomas or gangliogliomas) with a markedly more favorable course of survival, sometimes for years or decades (2, 3). DIPGs of the ventral pons peak in incidence in middle childhood (at the age of 6–7 y) and are rare in adulthood (3, 4) (Fig. 1*B*). The region- and age-specific nature of brainstem gliomas suggests that the underlying pathophysiology involves dysregulation of a postnatal neurodevelopmental process.

Neural stem cells, defined as cells with the capacity for self-renewal and production of multipotential progeny, are well recognized in the postnatal forebrain and spinal cord (5). For example, adult stem cell populations in the postnatal lateral ventricle subventricular zone contribute to olfactory bulb neurogenesis throughout life, and progenitors in the postnatal hippocampus produce granule cell layer neurons throughout life (5, 6). The presence of stem cells throughout the ventricular system of the neuroaxis has been described (7), but little attention has been paid to those in the subventricular zone of the third and fourth (IVth) ventricles. In addition to multipotent stem cells, important populations of more differentiated neural precursor cells exist throughout the central nervous system but are similarly underexplored in the brainstem.

The relationship of normal neural stem cells to so-called "cancer stem cells" (CSCs) is somewhat controversial, but there is an emerging view that certain brain tumors might arise from stem-like precursor cell populations in both children and adults (8–10). CSCs or tumor-initiating cells, isolated from primary brain tumors, possess many of the characteristics of normal neural stem cells, generate neurospheres in vitro, and can recapitulate the tumor in vitro and in vivo, whereas other cell types from the tumor cannot (8, 11). The glioma-initiating cells studied to date, isolated from other types of glial tumors, resemble normal neural stem cells in some respects, such as immunophenotype and molecular gene expression (8, 12, 13).

The clinical behavior of DIPG suggests it is a unique disease, distinct from typical high-grade gliomas occurring elsewhere in the central nervous system. The study of DIPG biology has been limited by a dearth of available tumor tissue, however. Biopsy of this tumor is rare, because the diagnosis can typically be made by MRI appearance alone and brainstem surgery poses a significant risk of morbidity. With little human tissue available for study and no realistic animal models, few published studies address the underlying biology of DIPG and no advances in treatment have occurred since the application of radiation therapy 35 y ago (4, 14).

Results

Nestin$^+$ and Olig2$^+$ Cell Populations in the Developing Human Ventral Pons. The spatial and temporal specificity of brainstem tumors (Fig. 1 *A* and *B*) prompted a close examination of the spatial and temporal distribution of neural precursor cells in the human brainstem throughout postnatal life. To accomplish this, 24 normal postmortem brainstem samples from all three brainstem regions—midbrain, pons, and medulla (Fig. 1*A*)—were analyzed from subjects lacking evidence of neurological, developmental, or oncological disease.

Immunohistochemical analysis and confocal microscopy revealed two distinct Nestin-immunopositive cell populations in the postnatal human brainstem: one population in the subventricular zone (defined as 50 μm deep to the ependymal layer) of the floor of the IVth ventricle and one population in the ventral pons. The ventral pontine Nestin$^+$ cells exhibit a distinct morphology, with

Author contributions: M. Monje, M.E.F., M.S.B.E., P.G.F., I.L.W., D.H.R., H.V., and P.A.B. designed research; M. Monje, S.S.M., M.E.F., T.B.R., J.K., M. Masek, T.H., and P.G.F. performed research; M. Monje, S.S.M., T.B.R., J.L.A., G.L., D.H.R., A.J.W., and P.A.B. contributed new reagents/analytic tools; M. Monje, S.S.M., M.E.F., J.K., H.V., and P.A.B. analyzed data; and M. Monje and P.A.B. wrote the paper.

The authors declare no conflict of interest.

Freely available online through the PNAS open access option.

[1]M. Monje and S.S.M. contributed equally to this work.

[2]To whom correspondence may be addressed. E-mail: mmonje@stanford.edu or pbeachy@stanford.edu.

[3]Present address: Section for Immunology, Institute for Experimental Medical Science, Lund University, 222 40 Lund, Sweden.

This article contains supporting information online at www.pnas.org/lookup/suppl/doi:10.1073/pnas.1101657108/-/DCSupplemental.

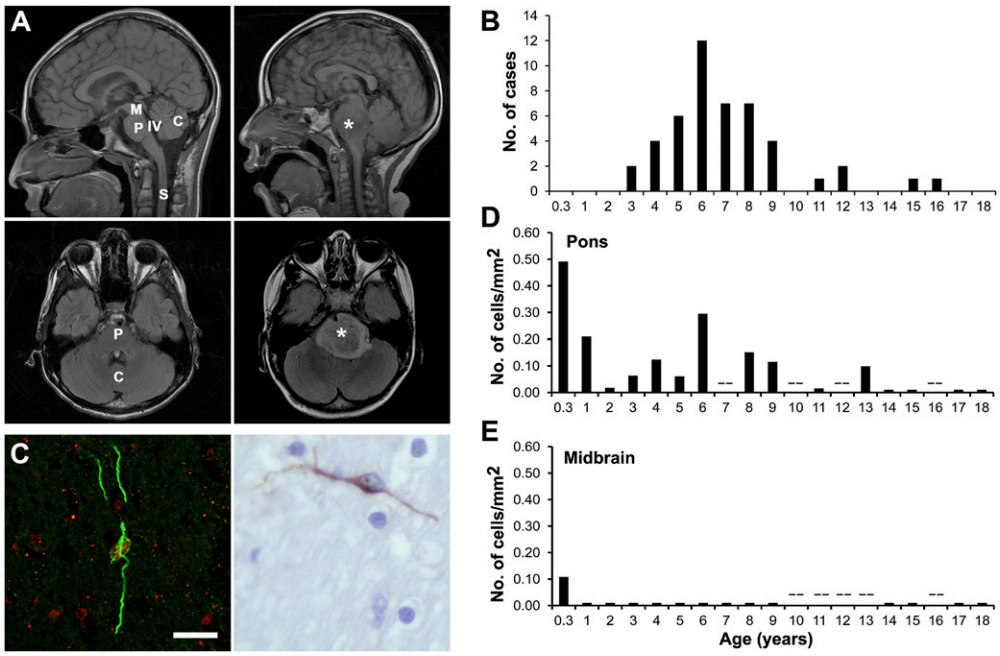

Fig. 1. Spatiotemporal distribution of ventral pontine PPCs and incidence of DIPG. (*A*) Sagittal and axial MRI scans showing normal brainstem anatomy (*Left*) and DIPG (*Right*). The DIPG tumor is indicated by an asterisk. C, cerebellum; M, midbrain, P, pons, S, spinal cord; IV, fourth ventricle. (*B*) Incidence of DIPG expressed at age of diagnosis. Data were drawn from the Stanford University Brain Tumor Database and represent all patients with DIPG cared for at Stanford University Medical Center from 1997–2008 (n = 47). (*C*) Ventral PPC visualized on confocal micrograph [*Left*; Nestin (green) and Olig2 (red), magnification 40×] and light micrograph [*Right*; Nestin (brown), magnification 60×]. (Scale bar: 50 μm.) Density of Nestin$^+$ cells in the human ventral pons (*D*) and midbrain (*E*) as a function of postnatal age (n = 24). Each data point represents one to two cases; when two cases are represented, the value expressed is an average of the two. The symbol (--) denotes an age at which no valid tissue samples were available for analysis. Comparable data in the medulla are presented in Fig. S1*E*.

long thin processes in a bipolar arrangement (Fig. 1*C*). These Nestin$^+$ cells also express the primitive neural precursor cell marker Vimentin but not GFAP (Fig. S1 *A* and *B*). In contrast, immunophenotypic neural precursor cells of the floor of the IVth ventricle subventricular zone do not uniformly coexpress Nestin and Vimentin (Fig. S1*C*). Approximately half (40–60%) of the Nestin$^+$/Vimentin$^+$ ventral pontine cells also express the basic helix–loop–helix transcription factor Olig2 (Fig. 1*C*), a marker frequently found in cells that ultimately give rise to oligodendroglial precursors. This cell type is morphologically distinct from Nestin$^+$ cells of the subventricular zone of the IVth ventricular floor, located in dorsal regions of the brainstem (Fig. S1 *C* and *D*).

The density of this Nestin$^+$ cell type in the human midbrain, pons, and medulla was quantified throughout childhood (Fig. 1 *D* and *E* and Fig. S1*E*). During infancy, this cell type is present in all ventral brainstem structures and then wanes by 2 y of age. In the human pons, this cell type again increases in density in middle childhood, peaking around the age of 6 y. This second peak in the ventral pontine Nestin$^+$ population corresponds strikingly with the incidence of DIPG (Fig. 1 *B* and *D*). A similar temporal distribution was observed in the medulla (Fig. S1*E*). In contrast, no such Nestin$^+$ cell population is seen in the midbrain after infancy (Fig. 1*E*).

Hedgehog Signaling Drives Proliferation of Olig2$^+$ Cells in the Murine Ventral Pons. Given the experimental limitations of human tissue, we investigated the occurrence of a correlate pontine precursor-like cell (PPC) population in the mouse. A caveat that should be noted is that murine brainstem anatomy (Fig. 2*A*) does not exactly mirror human brainstem anatomy. For example, some structures present in human medulla, such as the dorsal vagal complex, are instead found in the murine pons. We found Nestin$^+$ cells in the ependymal and subventricular zone of the murine IVth ventricular floor, similar to the floor of the human IVth ventricle. Nestin$^+$ and Vimentin$^+$ cells were extremely rare in the ventral murine brainstem at any time point during postnatal life, however. Nevertheless, we found a robust population of Olig2$^+$ cells in the far ventral pons (Fig. 2*B* and Fig. S2*A*), and some of these cells also expressed SOX2, a marker of primitive cell types (13) (Fig. S2*A*), suggesting precursor cell identity.

The Hedgehog (Hh) pathway is of interest in these candidate PPCs because of its established role in the physiology of other ventral neural precursor cell populations (15) and because Olig2 is known to be regulated in ventral embryonic spinal cord by Sonic hedgehog (Shh) (16). We therefore used a reporter for Hh pathway activity in which β-galactosidase is expressed under control of the promoter of the Hh pathway target, *Gli1* (*Gli1::LacZ*), and found expression of β-galactosidase concentrated in the far ventral pons (Fig. 2*C*). On closer examination, we found that all β-galactosidase$^+$ ventral pontine cells are also dual-positive for Olig2 and SOX2 expression (Fig. 2*B* and Fig. S2*A*). These Hh-responsive cells emerge around postnatal day (P) 14 and increase dramatically in this region from P14 to P21 (Fig. 2*D*), a time period in the mouse that roughly corresponds to "middle childhood" in humans, based on eye and tooth development. Unbiased stereological quantification reveals a three-fold increase in the total number of Hh-responsive cells in the ventral pons from P14 to P21 (Fig. 2*E*; 5,011 ± 373 at P14 vs. 14,599 ± 812 at P21, n = 4 animals per group; $P < 0.001$). These β-galactosidase$^+$ cells in the ventral pons do not coexpress the proliferation marker Ki67 but are intermixed with cells that are copositive for Ki67 and the oligodendrocyte precursor marker PDGF receptor-α (PDGFR-α) (Fig. S2*B*). On the basis of their location and time of emergence, these murine PPCs thus resemble human PPCs (*Discussion*).

Because of the established role for Hh signaling both in normal neural precursor cells (9, 15, 17, 18) and in other brain tumors, such as medulloblastoma (19–22), we postulated that the Hh pathway might play a role in transformation of this ventral PPC population. To test the functional and possibly oncogenic role of the Hh pathway in ventral pontine Olig2$^+$ precursor cells, we used a genetic mouse model in which the Hh pathway is specifically up-regulated in Olig2$^+$ cells. An *Olig2-Cre* mouse was crossed to a Rosa26-*flox-stop-flox-SmoothenedM2* (*R26-lsl-SmoM2*) mouse, such that Cre recombination results in expression of the constitutively active SmoothenedM2 protein, thus constitutively activating the Hh pathway in cells expressing Olig2 and their progeny. In this *Olig2-Cre; R26-lsl-SmoM2* mouse, we observed a 2.8-fold increase in the absolute number of proliferating cells in the ventral pons at P14 detected by Ki67 immunohistochemistry and quantified using unbiased stereology (Fig. 2 *F* and *G*; 18,728 ± 1,887 in control mice vs. 51,757 ± 3,434 in *Olig2-Cre; R26-lsl-SmoM2* heterozygous mice, n = 3 animals per group; $P < 0.005$). As in control littermates and in the *Gli1-*

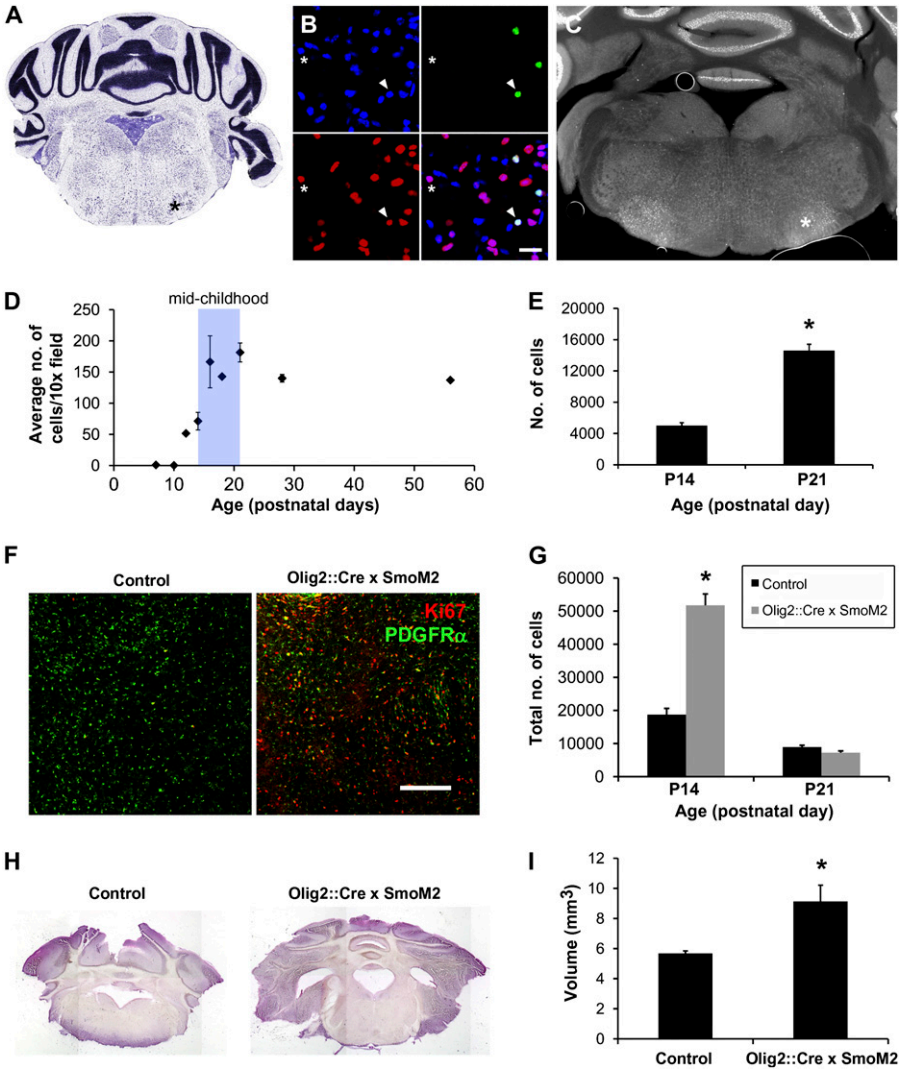

Fig. 2. Hh pathway is sufficient to drive proliferation in the ventral pons during middle childhood. (*A–E*) Hh-responsive Olig2$^+$ cells in the murine pons. (*A*) Nissl stain of the mouse pons Allen Mouse Brain Atlas (Seattle, WA): Allen Institute for Brain Science. ©2009. Available at http://mouse.brain-map.org (36). Region of Hh-responsive Olig2$^+$ precursor cells is marked with an asterisk. (*B*) Confocal photomicrograph (magnification 40×) illustrating colocalization of Olig2 (red) and β-galactosidase [indicating Gli1 expression (green)] in the *Gli1::LacZ* reporter mouse. DAPI expression (blue) is also shown. An arrowhead marks an example of an Olig2- and β-galactosidase–colabeled cell; an asterisk marks an example of a cell that is not colabeled. (*C*) Fluorescent micrograph (magnification 2.5×) showing Hh-responsive cells (white) in the *Gli1::LacZ* mouse. Note the cluster of Hh-responsive cells in the ventral pons (*). (*D*) Middle childhood peak in Hh-responsive cell density in the pons of the *Gli1::LacZ* transgenic reporter mouse. Data are expressed as the number of β-galactosidase–immunopositive cells per 10× field. Note the dramatic increase in Hh-responsive cells in the P14–P21 time frame, which represents the mouse equivalent of middle childhood. Data are mean ± SEM (n = 3 animals per time point). (*E*) Unbiased stereological quantification of the total number of Hh-responsive cells on one side of the ventral pons on P14 compared with P21. Data are mean ± SEM (n = 3 animals per time point; *$P < 0.001$). (*F* and *G*) Hh pathway activity increases proliferation in the ventral pons. (*F*) Confocal photomicrographs (magnification 10×) of Ki67$^+$ cells (red) in control and Olig2::Cre × SmoM2 heterozygote mouse ventral pons at P14. PDGFR-α (green) is shown. (Scale bar: 20 μm.) (*G*) Unbiased stereological quantification of Ki67$^+$ cells in the ventral pons at P14 in the *Olig2::Cre* × *SmoM2* mouse pons vs. littermate controls. Data are mean ± SEM (n = 3 animals per group; *$P < 0.005$). (*H* and *I*) Hh pathway upregulation results in ventral pontine hypertrophy. (*H*) Light micrographs (magnification 1.5×) of the ventral pons at P21 from *Olig2::Cre* × *SmoM2* heterozygote and littermate control mice. Images shown represent a reconstruction of the entire coronal brain section from multiple images taken at 1.5× magnification. (*I*) Volume of the ventral pons at P21 in *Olig2::Cre* × *SmoM2* heterozygotes vs. littermate controls. Data are expressed as the dorsal – ventral dimension × transverse dimension × rostrocaudal dimension in cubic millimeters. Data are mean ± SEM (n = 3 animals per group; *$P < 0.05$).

LacZ mice, proliferation at P14 in the *Olig2-Cre; R26-lsl-SmoM2* heterozygous mice was largely limited to this ventral pontine germinal zone and to PDGFR-α$^+$ oligodendrocyte precursor cells (Fig. 2*F*; the proportion of dividing cells that coexpress PDGFR-α and Ki67 was 88 ± 3% in *Olig2-Cre; R26-lsl-SmoM2* mice vs. 84 ± 5% in control mice; $P = 0.49$). This burst of proliferation in the ventral pons of *Olig2-Cre; R26-lsl-SmoM2* heterozygous mice ends by P21; at that time, unbiased stereological quantification of Ki67$^+$ cells reveals equal numbers of proliferating cells in control and *Olig2-Cre; R26-lsl-SmoM2* heterozygous mice (Fig. 2*G*; 9,696 ± 541 in control mice vs. 7,224 ± 543 in *Olig2-Cre; R26-lsl-SmoM2* heterozygous mice, $n = 3$ animals per group; $P = 0.09$).

By P21, hypertrophy of the ventral pons was evident in the *Olig2-Cre; R26-lsl-SmoM2* mice compared with control littermates (Fig. 2*H*). Measurement of the dorsal-ventral, transverse, and rostrocaudal dimensions of the pons in a one in four series of 40-μm tissue sections revealed an increase in volume of 50% (Fig. 2*I*; $P < 0.05$). Histological analysis on H&E-stained sections did not reveal dysplasia at P21 (Fig. S2*C*). Because these mice develop medulloblastoma during the postnatal period (10), all analyses carefully excluded regions of frank medulloblastoma present in the cerebellum and subarachnoid space, and careful examination of the pons at P14 and P21 revealed no infiltration of the brainstem by medulloblastoma cells. These mice die of medulloblastoma in early adulthood, thereby limiting later analysis of dysplasia in the pons.

Establishment of Previously Undescribed DIPG Cell Culture and Xenograft Models. A major obstacle in the study of DIPG has been a lack of available tumor tissue for research. To overcome this impasse, an early postmortem tissue harvest strategy was used. DIPG tumor tissue was donated by a 5-y-old boy who had received minimal treatment (clinical details are presented in *SI Materials and Methods*). Histopathology was consistent with a WHO grade III anaplastic astrocytoma (Fig. 3 *A*, *C*, *E*, *G*, and *I* and Fig. S3 *A*, *B*, and *F*) that was intensely immunopositive for Nestin (Fig. S3*A*) and GFAP (Fig. S3*F*).

Cells cultured on a nonadherent plate in serum-free medium supplemented with FGF and EGF formed tumor neurospheres (Fig. 4*A*) and secondary tumor neurospheres after dissociation and replating at low density (10 cells/μL). Limiting dilution analysis (23) of unsorted cells indicated an in vitro self-renewing frequency of 1 in 79 cells (1 in 64–1 in 98 cells, 95% confidence interval). Subsequent supplementation of PDGF-AB to the medium resulted in qualitative improvement of neurosphere

culture growth; the neurosphere culture expanded more rapidly after this addition, but the change in growth rates was not quantified at the time.

Using cultures with a low passage number (<10), the immunophenotype of neurosphere-forming cells was assessed using fluorescent immunocytochemistry and confocal microscopy. We found that all cells in the culture expressed the intermediate filament proteins Nestin, GFAP, and Vimentin (Fig. 4 *B* and *C*), which are classically found in neural stem or precursor cells and more recently described in many glial tumors (24). Nestin and Vimentin also mark endothelial cells, which is a potential source of culture contamination. Endothelial cells, however, were not present as assessed by immunostaining or FACS analysis for the endothelial cell-specific marker CD31. Sox2, a marker expressed in both normal embryonic and postnatal stem cells and in poorly differentiated CSCs (13), was also expressed to varying degrees in all DIPG neurosphere cells (Fig. 4*D*). A small subset of cultured DIPG neurosphere cells express Olig2 (Fig. 4*F*). Taken together, this immunophenotype of cultured DIPG neurosphere cells is consistent with a primitive neural precursor cell type.

Brain tumor-initiating cells are classically identified with the cell surface marker CD133 (also known as prominin 1 or Prom1) (11). Recently, it has become clear that CD133 may only mark a subset of the self-renewing cancer-propagating cells in a glioma (25). CD133 is also expressed on normal neural stem cells, although the expression of CD133 is similarly nonuniform in normal neural stem cells and may be restricted to the actively proliferating fraction of stem cells (26). Increasing $CD133^+$ fractions of brain tumor cultures correlates with higher tumor grade (11). Examining the proportion of cells in the DIPG neurosphere culture that express CD133, we found that 37% of cells are $CD133^+$ by FACS (Fig. S3*C*) and that a similar fraction are positive by immunocytochemistry (approximately one-third of cells, Fig. 4*E*). Examination of the original tumor tissue revealed $CD133^+$ cells sparsely distributed throughout the tumor (Fig. S3*B*).

To test for tumor-initiating capacity and to establish a xenograft mouse model, dissociated neurosphere cells were stereotactically transplanted to the brains of immunodeficient (nonobese diabetic/SCID/IL2γ-chain–deficient) mice on P2. Two transplantation strategies were used, and cells were transplanted either to the lateral ventricles (LV, three mice) or to the IVth ventricle (IV, eight mice). Mice were routinely examined for neurological deficits. Twenty-six weeks following neurosphere cell transplantation, all three mice in the LV group and four of eight mice in the IV group exhibited clinical symptoms, such as poor grooming and hemiparesis. Two-thirds of the mice from both groups were sacrificed, and the brains were processed for histology; one-third of the mouse brains were processed for serial transplantation of the xenograft. In the LV group, all brains demonstrated large tumors, evident by eye (Fig. 3*B*) and on H&E-stained sections (Fig. 3 *D* and *F* and Fig. S3 *D* and *H*). Tumor histopathology was characteristic of a high-grade glioma (Fig. 3 *D* and *F* and Fig. S3 *D*, *E*, *G*, and *H*). Infiltrating tumor cells were found throughout the mouse brain, including the cortex, cerebellum, and pons (Fig. 3 *D* and *F* and Fig. S3 *D* and *H*). Invasion of the brainstem following LV tumor cell injection has not been observed by our group in this orthotopic mouse transplant model with any other tumor type, including multiple cases of glioblastoma and medulloblastoma. This highlights the unique biology of DIPG, as distinct from other high-grade gliomas. In the IVth ventricle group, 50% of brains exhibited tumors evident by eye as enlarged hindbrains and histologically on H&E-stained sections (Fig. 3 *H* and *J* and Fig. S3*I*). Like the LV xenografted brains, diffuse infiltration of the brainstem, cerebellum, and cerebrum was observed (Fig. 3 *H* and *J* and Fig. S3*I*). In comparison with xenografts to the LVs, xenografting to the IVth ventricle resulted in pontine histopathology more similar to that of DIPG (Fig. 3*F* vs. *H* and *J*).

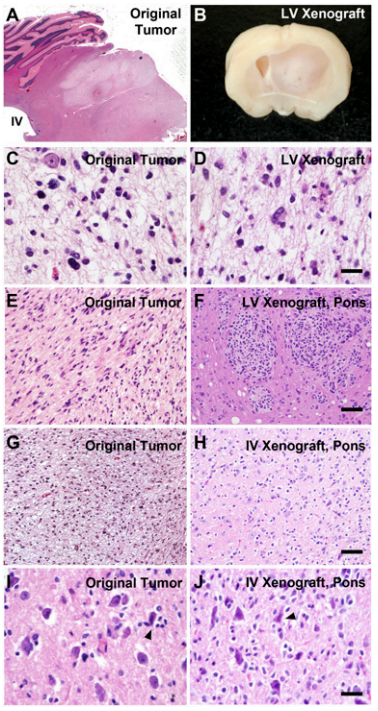

Fig. 3. DIPG xenograft. H&E-stained light micrographs (*A*, *C–J*) and bright-field image of mouse brain (*B*). (*Left*) Original DIPG tumor. (*A*) Light micrograph (magnification 2×) of H&E-stained sagittal section through the pons of the tumor tissue donor. Diffuse infiltration of tumor in the ventral pons is visualized as lighter staining, notably sparing the dorsal region of pons that is closest to the IVth ventricle. The cerebellum is seen in the dorsolateral relationship to the pons in this plane of section. Additional images of the original tumor are shown at magnifications of 40× (*C* and *I*), 20× (*E*), and 10× (*G*). (*Right*) Mouse DIPG xenografts. (*B*) Following stereotactic transplantation of dissociated neurospheres from a human DIPG to the LV, examination of brains from immunodeficient mice reveals a large tumor and marked midline shift evident on a gross coronal section. (*D*) Diffuse infiltration by tumor is seen throughout the brain in H&E-stained sections (magnification 40×). (*F*) Although the DIPG cells were transplanted to the LVs, infiltration was seen in the hindbrain, including the pons (magnification 20×). (*H* and *J*) Transplantation of dissociated neurospheres from a human DIPG to the IVth ventricle resulted in diffuse infiltration of the pons. Note the perineuronal satellitosis (arrowheads) of tumor cells around pontine neurons (larger cells) seen in the xenograft (*J*) and original tumor (*I*). The histopathology of the mouse xenograft was indistinguishable from that of the original tumor. (Scale bars: *C*, *D*, and *I–J*, 50 μm; *E–H*, 100 μm; G and *H*, 250 μm.)

Functional Role for Hh Signaling in DIPG. Using the newly established DIPG cell culture model, we tested the role of Hh signaling in human DIPG. To test for Hh pathway activity, a Gli reporter construct was used in which red fluorescent protein (RFP) expression is under control of Gli binding sites within a lentiviral vector. To validate this Hh pathway reporter system, National Institutes of Health (NIH) 3T3 cells were transduced with the Gli binding site::RFP reporter and exposed to the Shh protein ligand (ShhN) alone or together with the Hh antagonist 3-keto-*N*-(aminoethyl-aminocaproyl-dihydrocinnamoyl)-cyclopamine (KAAD-cyclopamine, 200 nM). At baseline, NIH 3T3 cells did not express RFP (Fig. S4*A*), but RFP was expressed in transduced NIH 3T3 cells when exposed to ShhN (Fig. S4*B*). RFP expression in transduced NIH 3T3 cells exposed to ShhN was blocked by simultaneous exposure to KAAD-cyclopamine (Fig. S4*C*).

Dissociated DIPG neurosphere cells from the initial culture described above, as well as primary tumor cells from a second tumor tissue donation, were transduced with lentivirus containing either the WT Gli binding site-RFP construct (Fig. 5*A*) or a negative control construct with mutated Gli binding sites (Fig. 5*B*). As a positive control, 293 cells expressing Gli1 were also transduced with the Gli binding site-RFP reporter construct. RFP expression indicated Hh pathway activity in both the primary DIPG tumor cell culture and the dissociated neurosphere cells (Fig. 5*A*). To determine the source of Hh ligand in this culture, immunocytochemistry for Shh was performed. DIPG neurosphere cells uniformly

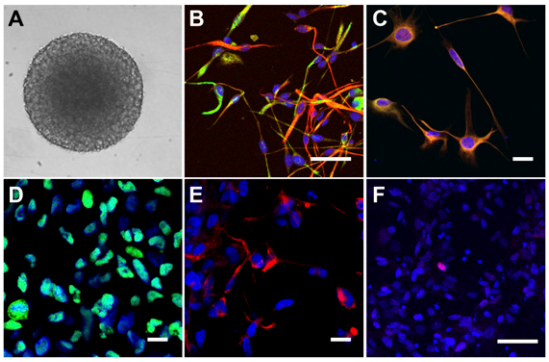

Fig. 4. DIPG neurosphere culture. (*A*) Tumor neurosphere is shown on a light micrograph (magnification 10×). Immunocytochemistry and confocal microscopy (magnification 40×) reveal DIPG tumor neurosphere cells that are uniformly immunopositive for GFAP (*B*, red), Nestin (*B* and *C*, green) Vimentin (*C*, red), and Sox2 (*D*, green). Immunocytochemistry for CD133 (*E*, red) reveals a CD133$^+$ fraction of about one-third of cells. Rare cells are immunopositive for Olig2 (*F*, red). DAPI (blue) was used as a nuclear counterstain in images *B*–*F*. (Scale bars: 50 μm.)

express Shh ligand, indicating an autocrine and/or paracrine Hh signaling mechanism (Fig. 5*C*). Semiquantitative real-time RT-PCR confirmed expression of Gli1, Patched (PTCH) receptor, and Shh ligand in DIPG neurosphere cells (Fig. S4*D*).

To test the functional significance of the Hh pathway on DIPG tumor neurosphere cell self-renewal capacity, we used a secondary neurosphere assay. Dissociated DIPG tumor neurosphere cells were plated at low density (100 cells per well in a 96-well plate format) using FACS sorting of live cells and then cultured in the presence or absence of added processed and purified Shh (ShhNp) or the Hh pathway antagonist KAAD-cyclopamine. Neurosphere formation (Fig. 5*D*) was quantified at 14 d following plating of dissociated cells. Exposure to KAAD-cyclopamine (200 nM) resulted in a 67% reduction in the average number of secondary neurospheres per well ($P < 0.001$) compared with control wells treated with methanol vehicle alone (Fig. 5*E*). The addition of ShhNp increased secondary neurosphere formation by 200% ($P < 0.05$; Fig. 5*E*).

Discussion

DIPGs are aggressive tumors of childhood that are poorly understood and nearly always fatal. The lack of a faithful experimental model system together with a limited understanding of the normal neural precursor cell biology of the postnatal brainstem has limited study of this devastating disease and prevented development of effective treatment strategies.

We now report the identification of a neural precursor-like cell population in the normal human ventral pons that is linked both anatomically and temporally to the incidence of DIPG (Fig. 1). The frequency of this cell type during middle childhood mirrors the bell-shaped incidence curve of DIPG (Fig. 1 *B* and *D*). These cells are notably absent after early infancy in the midbrain (Fig. 1*E*), where high-grade gliomas are virtually nonexistent. This PPC is restricted to the ventral pons and medulla during childhood (Fig. 1*D* and Fig. S1*E*). High-grade gliomas primarily occur in the ventral pons but are sometimes found in the medulla as well. The predilection for the ventral pons may reflect not only the presence of a susceptible cell of origin but a signaling microenvironment favorable for tumor formation (27–29). Differences in brainstem cell populations and in their behavior may relate to the different developmental origins of each brainstem region, with the human midbrain, pons, and medulla arising from three different neuroembryonic vesicles (the mesencephalon, metencephalon, and myelencephalon, respectively).

The human PPC population comprises primitive Nestin$^+$ and Vimentin$^+$ cells with long bipolar processes (Fig. 1*C* and Fig. S1 *A* and *B*), with a significant subset of these cells coexpressing Olig2 (Fig. 1*C*). We note that although coexpression of Nestin with Olig2 occurs in this human cell population, coexpression of these two markers has not previously been described and appears not to occur in the mouse. The Olig2$^+$ precursor population that we have found in the mouse ventral pons does not express Nestin, and the murine correlate to this human PPC that we have characterized is thus similar but not identical in a manner consistent with precedent. Olig2$^+$ precursor cells frequently represent cells that ultimately form myelinating oligodendroglia, although differentiation along astroglial and even neuronal lineages is also described (30). In the mouse, Hh-responsive Olig2$^+$ precursors in the ventral pons are intermixed with dividing PDGFR-α–immunopositive oligodendrocyte precursor cells (Fig. S2*B*), suggesting that this population forms myelinating oligodendrocytes during middle childhood (P14–P21 in the mouse). The majority of postnatal myelination is complete by this time point, but ongoing myelination is known to occur in the human pons through the first decade of life (31). The precise tracts that are myelinating and why this may occur specifically during middle childhood are unknown.

Similar to human PPCs, DIPG neurosphere cells are Nestin$^+$ and Vimentin$^+$, with a subset expressing Olig2 (Fig. 4 *C* and *F*). In contrast to the normal human PPC, the DIPG tumor neurosphere cells also express GFAP (Fig. 4*B*), a marker expressed in many glial tumors regardless of the cell of origin (32). Taken together with the anatomical and temporal correlates of their occurrence, the immunophenotypic characteristics of these cell populations suggest the hypothesis that this PPC could be the DIPG cell of origin.

Our results show that driving unregulated Hh pathway activity in the murine counterpart of this population results in ventral pontine hyperplasia (Fig. 2 *F*–*I*), indicating that the PPC might be susceptible to transformation and may represent the cell of origin for DIPG. The absence of dysplasia in this model suggests that an additional "hit" may be necessary for transformation to DIPG. That Hh pathway dysregulation alone may not be sufficient for DIPG oncogenesis is supported by the observation that patients with Gorlin syndrome (a genetic syndrome of susceptibility to unregulated Hh pathway activity caused by heterozygous germline mutation of the PTCH gene and characterized by de-

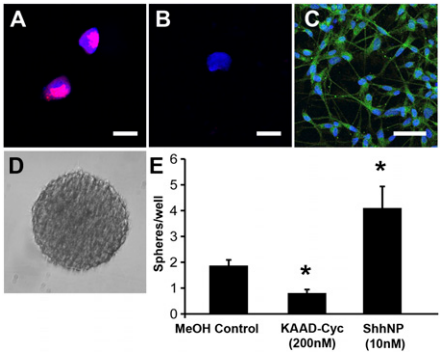

Fig. 5. Hh pathway activity in DIPG. (*A*) DIPG tumor cells transduced with a lentiviral Hh pathway reporter construct, Gli1::RFP. A confocal photomicrograph (magnification 40×) illustrates RFP (red) and a DAPI nuclear counterstain (blue). (*B*) Confocal photomicrograph (magnification 40×) illustrates lack of RFP (red) signal in negative control tumor cells transduced with a mutated Gli1 binding site::RFP construct and a DAPI nuclear counterstain (blue). (Scale bar: 30 μm.) (*C*) Confocal photomicrograph (magnification 40×) demonstrates Shh ligand expression (green) in DIPG tumor neurosphere cells. A DAPI nuclear counterstain (blue) is also shown. (*D*) Light micrograph (magnification 10×) of a secondary tumor neurosphere at 14 d following dissociation and FACS sorting of live cells at low density (100 cells per well in a 96-well plate format). (*E*) Quantification of secondary tumor neurospheres (such as that seen in *D*) at 14 d following dissociation and FACS sorting of live cells at low density (100 cells per well) and exposed to either KAAD-cyclopamine (200 nM), ShhNp (10 nM), or methanol vehicle control. Data are expressed as the average number of tumor neurospheres per well ± SEM (n = 10–16 wells per condition; *$P < 0.05$).

velopment of basal cell nevi and medulloblastoma) do not classically develop DIPG. Our results indicate that the Hh pathway is one important component in both the normal physiology of the PPC and the pathophysiology of DIPG, because Hh pathway activation increases and Hh pathway blockade decreases the self-renewal capacity of cells in DIPG tumor neurospheres (Fig. 5*E*).

Dysregulation of the Hh pathway alone is not enough to cause both hyperplasia and dysplasia (i.e., cancer) in the ventral brainstem by P21 in the mouse model used here, as we also previously reported (10), and transformation to DIPG likely involves additional hits. Indeed, recent work has highlighted the PDGF pathway as important in brainstem tumors, with genomic analysis of DIPG samples demonstrating copy number alterations in PDGFR-α (33). In addition, up-regulation of PDGF signaling in Nestin$^+$ cells of the IVth ventricle subventricular zone (22) or nonspecifically in cells of the dorsolateral pons (34) causes dorsal pontine glioblastoma in mouse models. A putative role for PDGF signaling in DIPG pathophysiology fits well with our observations, because the candidate cell of origin appears to give rise to a dividing oligodendrocyte precursor cell type that expresses PDGFR-α, and is therefore likely to be responsive to PDGF. Furthermore, we found qualitatively that the addition of recombinant PDGF to our human DIPG cell culture resulted in improved culture yield.

We present here a postmortem cell culture strategy that has generated DIPG culture and xenograft models (Figs. 3 and 4), representing a previously undescribed resource for the research community and enabling studies to probe the underlying biology of DIPG. Within this DIPG cell culture, we have demonstrated a capacity for self-renewal and tumor initiation as well as an immunophenotype similar to that of a neural stem cell, suggesting the presence of a putative DIPG CSC. The characteristics of this neurosphere culture are consistent with those of an aggressive brain tumor, because a CD133$^+$ cell fraction of 37% is relatively high compared with that previously reported for other aggressive brain tumors, such as medulloblastoma and glioblastoma (6–21% and 19–29%, respectively) (35). Adjusting for the enrichment of CD133$^+$ cells by FACS in published secondary neurosphere assays, the self-renewing frequency found in this study (1 in 79 cells) is in line with that of similar studies of medulloblastoma tumor neurospheres (11).

The human PPC population we have described is temporally and anatomically restricted to the time and place that DIPGs form and is immunophenotypically similar to DIPG, suggesting that this cell is a candidate for the DIPG cell of origin. This hypothesis is strengthened by the demonstration that up-regulation of the Hh pathway in mouse ventral PPCs results in ventral pontine hyperplasia during the middle childhood window when such tumors form in humans. A role for Hh signaling in DIPG tumor propagation is confirmed by the positive effects of Hh pathway activity on self-renewal of DIPG neurosphere cells in our DIPG cell culture model. Together, these findings provide insights into DIPG pathogenesis and may ultimately result in unique therapeutic avenues to treat DIPG.

Materials and Methods

Full methodological details are found in the *SI Materials and Methods* including methods for cell culture, xenografting, archival human autopsy case selection and quality control, histological processing, quantitative microscopy, FACS analysis, generation of the lentiviral-based Gli binding site-RFP reporter, real time PCR and statistics. Clinical details of the human postmortem tissue donation are also provided.

ACKNOWLEDGMENTS. We thank Arturo Alvarez-Buylla, Sandy Smith, Kimberlee Spady, and Jason Karamchandani for their help with the manuscript. We gratefully acknowledge the generous support of the Kyle O'Connell Foundation (M.S.B.E. and M. Monje), Dylan Jewett Family Fund (M. Monje), Reid Ebrom Family Fund (M. Monje), Sence Foundation (M. Monje and P.G.F.), Childhood Brain Tumor Foundation (P.A.B.), Pediatric Brain Tumor Foundation (J.L.A., T.B.R., I.L.W., and D.H.R.), National Brain Tumor Foundation (A.J.W.), and Howard Hughes Medical Institute (P.A.B. and D.H.R.). This study was also supported by National Institutes of Health Grants 1K08NS070926-01 (to M. Monje), CA69495 (to A.J.W.), and CA124832 (to A.J.W.); and by Stanford Cancer Center Developmental Cancer Research Awards (to I.L.W. and T.B.R.).

1. Central Brain Tumor Registry of the United States (2010) *CBTRUS Statistical Report: Primary Brain and Central Nervous System Tumors Diagnosed in the United States in 2004-2006* (Central Brain Tumor Registry of the United States, Hinsdale, IL).
2. Barkovich AJ, et al. (1990-1991) Brain stem gliomas: A classification system based on magnetic resonance imaging. *Pediatr Neurosurg* 16:73–83.
3. Fisher PG, et al. (2000) A clinicopathologic reappraisal of brain stem tumor classification. Identification of pilocystic astrocytoma and fibrillary astrocytoma as distinct entities. *Cancer* 89:1569–1576.
4. Donaldson SS, Laningham F, Fisher PG (2006) Advances toward an understanding of brainstem gliomas. *J Clin Oncol* 24:1266–1272.
5. Zhao C, Deng W, Gage FH (2008) Mechanisms and functional implications of adult neurogenesis. *Cell* 132:645–660.
6. Shors TJ, et al. (2001) Neurogenesis in the adult is involved in the formation of trace memories. *Nature* 410:372–376.
7. Weiss S, et al. (1996) Multipotent CNS stem cells are present in the adult mammalian spinal cord and ventricular neuroaxis. *J Neurosci* 16:7599–7609.
8. Hemmati HD, et al. (2003) Cancerous stem cells can arise from pediatric brain tumors. *Proc Natl Acad Sci USA* 100:15178–15183.
9. Yang ZJ, et al. (2008) Medulloblastoma can be initiated by deletion of Patched in lineage-restricted progenitors or stem cells. *Cancer Cell* 14:135–145.
10. Schüller U, et al. (2008) Acquisition of granule neuron precursor identity is a critical determinant of progenitor cell competence to form Shh-induced medulloblastoma. *Cancer Cell* 14:123–134.
11. Singh SK, et al. (2003) Identification of a cancer stem cell in human brain tumors. *Cancer Res* 63:5821–5828.
12. Taylor MD, et al. (2005) Radial glia cells are candidate stem cells of ependymoma. *Cancer Cell* 8:323–335.
13. Ben-Porath I, et al. (2008) An embryonic stem cell-like gene expression signature in poorly differentiated aggressive human tumors. *Nat Genet* 40:499–507.
14. Laigle-Donadey F, Doz F, Delattre JY (2008) Brainstem gliomas in children and adults. *Curr Opin Oncol* 20:662–667.
15. Ahn S, Joyner AL (2005) In vivo analysis of quiescent adult neural stem cells responding to Sonic hedgehog. *Nature* 437:894–897.
16. Lu QR, et al. (2000) Sonic hedgehog—Regulated oligodendrocyte lineage genes encoding bHLH proteins in the mammalian central nervous system. *Neuron* 25:317–329.
17. Lai K, Kaspar BK, Gage FH, Schaffer DV (2003) Sonic hedgehog regulates adult neural progenitor proliferation in vitro and in vivo. *Nat Neurosci* 6:21–27.
18. Breunig JJ, et al. (2008) Primary cilia regulate hippocampal neurogenesis by mediating sonic hedgehog signaling. *Proc Natl Acad Sci USA* 105:13127–13132.
19. Goodrich LV, Milenković L, Higgins KM, Scott MP (1997) Altered neural cell fates and medulloblastoma in mouse patched mutants. *Science* 277:1109–1113.
20. Pomeroy SL, et al. (2002) Prediction of central nervous system embryonal tumour outcome based on gene expression. *Nature* 415:436–442.
21. Ehtesham M, et al. (2007) Ligand-dependent activation of the hedgehog pathway in glioma progenitor cells. *Oncogene* 26:5752–5761.
22. Becher OJ, et al. (2010) Preclinical evaluation of radiation and perifosine in a genetically and histologically accurate model of brainstem glioma. *Cancer Res* 70:2548–2557.
23. Quintana E, et al. (2008) Efficient tumour formation by single human melanoma cells. *Nature* 456:593–598.
24. Ma YH, et al. (2008) Expression of stem cell markers in human astrocytomas of different WHO grades. *J Neurooncol* 86:31–45.
25. Clément V, Dutoit V, Marino D, Dietrich PY, Radovanovic I (2009) Limits of CD133 as a marker of glioma self-renewing cells. *Int J Cancer* 125:244–248.
26. Sun Y, et al. (2009) CD133 (Prominin) negative human neural stem cells are clonogenic and tripotent. *PLoS ONE* 4:e5498.
27. Gilbertson RJ, Gutmann DH (2007) Tumorigenesis in the brain: Location, location, location. *Cancer Res* 67:5579–5582.
28. Calabrese C, et al. (2007) A perivascular niche for brain tumor stem cells. *Cancer Cell* 11: 69–82.
29. Gilbertson RJ, Rich JN (2007) Making a tumour's bed: Glioblastoma stem cells and the vascular niche. *Nat Rev Cancer* 7:733–736.
30. Zhou Q, Anderson DJ (2002) The bHLH transcription factors OLIG2 and OLIG1 couple neuronal and glial subtype specification. *Cell* 109:61–73.
31. Yakovlev PI (1967) The myelogenetic cycles of regional maturation of the brain. *Regional Development of the Brain in Early Life*, ed Minkowski A (Blackwell Scientific, Oxford), pp 3–70.
32. Lindberg N, Kastemar M, Olofsson T, Smits A, Uhrbom L (2009) Oligodendrocyte progenitor cells can act as cell of origin for experimental glioma. *Oncogene* 28: 2266–2275.
33. Zarghooni M, et al. (2010) Whole-genome profiling of pediatric diffuse intrinsic pontine gliomas highlights platelet-derived growth factor receptor alpha and poly (ADP-ribose) polymerase as potential therapeutic targets. *J Clin Oncol* 28:1337–1344.
34. Masui K, et al. (2010) Glial progenitors in the brainstem give rise to malignant gliomas by platelet-derived growth factor stimulation. *Glia* 58:1050–1065.
35. Singh SK, et al. (2004) Identification of human brain tumour initiating cells. *Nature* 432:396–401.
36. Lein ES, et al. (2007) Genome-wide atlas of gene expression in the adult mouse brain. *Nature* 445:168–176.